crystals

MDPI

Article

Effect of Isothermal Cooling During Thermal Processes on Minority Carrier Lifetime of p-Type Czochralski Silicon

Panbing Zhou [1,*], Kun Wei [2], Ying Zhao [1] and Lang Zhou [3]

[1] School of New Energy and Vehicle Engineering, Nanchang Institute of Science and Technology, Nanchang 330108, China
[2] School of Mechanical and Robotics Engineering, Nanchang Institute of Science and Technology, Nanchang 330108, China
[3] Institute of Photovoltaics, Nanchang University, Nanchang 330031, China
* Correspondence: zhoupanbing@ncu.edu.cn

Abstract

This paper reports the study of how isothermal cooling—a physical metallurgical processing technique—affects interstitial iron concentration and minority carrier lifetime in p-type Czochralski silicon for photovoltaic applications. The experimental results demonstrate that thermal-induced degradation of minority carrier lifetime occurs in p-type Czochralski wafers subjected to isothermal holding across a range of temperatures following heating at 900 °C. Under identical heating conditions, varying the subsequent isothermal holding temperature reveals a clear extremum: interstitial iron concentration decreases monotonically as temperature rises from 450 °C up to 650 °C, reaching its minimum at 650 °C; conversely, minority carrier lifetime increases with temperature in this regime and peaks at 650 °C. Above 650 °C, interstitial iron concentration increases and minority carrier lifetime declines. Thus, isothermal holding at 650 °C optimizes iron precipitation—minimizing interstitial iron concentration while maximizing minority carrier life-time. Holding time-dependent experiments at 650 °C (holding durations: 0, 30, 60, 120, 180, and 240 min) further show that interstitial iron concentration decreases monotonically with increasing holding time, accompanied by a corresponding monotonic increase in minority carrier lifetime.

Keywords: Czochralski silicon; thermal processes; isothermal cooling; minority carrier lifetime; interstitial iron concentration

1. Introduction

Currently, Czochralski silicon (Cz-Si) serves as the dominant material for commercial solar cell production. Relative to the cast multicrystalline silicon produced via directional solidification, Cz-Si exhibits a significantly lower dislocation density, reduced metallic impurity concentration, and the absence of grain boundaries [1]—attributes that collectively contribute to superior photoelectric conversion efficiency in resultant solar cells. Moreover, ongoing process optimization and economies of scale have driven a sustained reduction in manufacturing costs [2]. Consequently, by the end of 2025, its global market share had exceeded 98% [3].

Minority carrier lifetime (τ) constitutes a critical performance metric for photovoltaic-grade crystalline silicon, directly governing the photoelectric conversion efficiency of silicon-based solar cells [4]. Enhancing this lifetime in the bulk material—or mitigating its degradation during solar cell fabrication—is therefore essential to achieving higher power conversion efficiencies. Our research group examined the influence of heating temperature and cooling

Check for updates

Academic Editor: Guanying Chen

Received: 2 October 2026
Revised: 14 November 2026
Accepted: 18 November 2026
Published: 25 November 2026

Copyright: © 2026 by the authors. Licensee MDPI, Basel, Switzerland. This article is an open access article distributed under the terms and conditions of the Creative Commons Attribution (CC BY) license.

rate on both τ and interstitial iron concentration ([Fei]) in heat-treated Cz-Si. The results demonstrate that heating samples within the range of 300–1050 °C followed by rapid cooling to ambient temperature at 50 °C/s induces a pronounced reduction in τ; moreover, the magnitude of degradation increases monotonically with rising heat temperature, as illustrated in Figure 1a [5]. Furthermore, when high-temperature heating (≥800 °C) is coupled with cooling rates spanning 0.017–50 °C/s, a higher cooling rate consistently correlates with greater lifetime attenuation, as illustrated in Figure 1b [5]. This thermally induced degradation of τ—is herein defined as thermal-induced degradation (TID) of τ in crystalline silicon. Independent studies corroborate this phenomenon: Buonassisi et al. [6] demonstrated that high-temperature thermal processing followed by rapid cooling induces performance degradation in silicon-based semiconductor defects—and therefore recommend prioritizing low-temperature annealing protocols coupled with controlled, gradual cooling in industrial fabrication whenever feasible. Rohatgi et al. [7] identified rapid cooling as a primary driver of deep-level trap formation in crystalline silicon, leading to measurable reductions in τ; critically, these thermally induced traps are reversible and can be effectively eliminated via subsequent low-temperature annealing or controlled gradual cooling. Similarly, research conducted by Xi et al. [8] reported that rapid cooling of monocrystalline silicon wafers significantly shortens minority carrier diffusion length—a direct consequence of TID of τ.

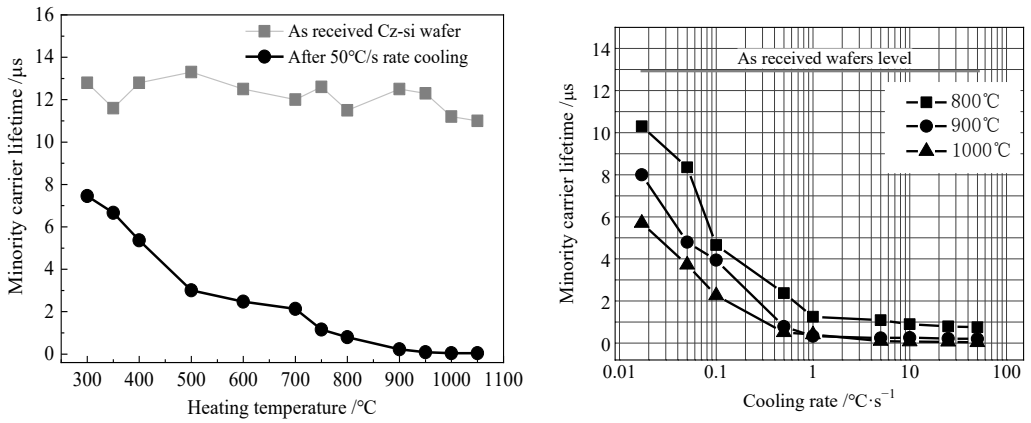


Figure 1. Effect of continuous cooling on minority carrier lifetime in Cz-Si. (**a**) Minority carrier lifetime after rapid cooling (50 °C/s) following heating at varying temperatures; (**b**) minority carrier lifetime after continuous cooling at controlled rates following heating at multiple temperatures [5].

The theoretical framework governing TID of τ in crystalline silicon is well established. Solar-grade Cz-Si commonly contains metallic impurities—including iron, copper, cobalt, and nickel—with iron being the most prevalent and electrically active transition-metal contaminant. This dominance arises from its relatively higher solid solubility in silicon, large non-radiative recombination cross-section, and frequent introduction during wafer handling and solar cell fabrication, particularly via direct contact with iron-containing tools, fixtures, and processing equipment [9,10]. In crystalline silicon, iron impurities predominantly reside in three thermodynamically distinct configurations: electrically active interstitial iron (Fe_i), complexes (notably FeB and FeAl), and metallic precipitates (e.g., α-$FeSi_2$ and β-$FeSi_2$) [6,11–13]. In p-type Cz-Si, interstitial iron atoms readily associate with substitutional boron dopants at ambient temperature to form stable FeB pairs [14]. Consequently, the dominant iron-related species present at ambient temperature are FeB complexes and iron-rich precipitates. Both the FeB complexes and iron precipitates introduce deep-level recombination centers within the silicon bandgap: the FeB complex exhibits an energy level located at E_c 2212x 0.29 eV [15–17] whereas iron precipitates introduce

a deep acceptor state at E_v + 0.63 eV [8]. These defect levels act as efficient Shockley–Read–Hall recombination centers, thereby substantially diminishing τ [12,13]. Owing to iron's extremely low equilibrium solid solubility in silicon, the slow cooling inherent to Czochralski crystal growth promotes extensive precipitation—yielding coarse, spatially isolated iron-rich particles. Such heterogeneous distribution effectively segregates iron from the active silicon matrix, thereby mitigating its detrimental impact on τ. However, upon thermal processing (e.g., annealing at elevated temperatures), these precipitates undergo partial or complete dissolution, releasing mobile Fe_i into the lattice. During subsequent rapid cooling (e.g., air quenching or forced convection cooling), kinetic constraints inhibit long-range diffusion and reprecipitation; consequently, a fraction of the liberated iron remains in solution as interstitial atoms. Upon cooling to ambient temperature, these atoms pair with boron within 24 h, yielding a uniform distribution of FeB complexes [1] (p. 130). Concurrently, residual supersaturation may drive nucleation of new precipitates—but under high cooling rates, enhanced nucleation density and suppressed growth kinetics favor formation of numerous nanoscale precipitates rather than coarse aggregates [6]. This dual-phase microstructure—comprising homogeneously dispersed FeB complexes and a high-density population of nanoscale iron precipitates—synergistically degrades minority-carrier diffusion length [6,18]. Supporting experimental evidence is provided by infra-red absorption mapping reported by Xi et al. [8]: wafers subjected to 1100 °C heating followed by rapid cooling (30 °C/s) exhibit fine, uniformly distributed iron precipitates, whereas identical wafers cooled slowly (0.3 °C/s) develop sparsely distributed, micron-scale precipitates—thereby corroborating the critical role of cooling kinetics in deter-mining iron speciation and associated electronic degradation.

During the fabrication of crystalline silicon solar cells, silicon wafers undergo key thermal processes such as phosphorus diffusion for p-n junction formation and electrode sintering. Phosphorus diffusion is typically conducted at temperatures ranging from 800 °C to 900 °C, while electrode sintering reaches peak temperatures of approximately 800 °C. Currently, major photovoltaic manufacturers primarily optimize these thermal parameters to satisfy discrete process-specific technical requirements, with limited consideration given to their influence on the intrinsic electrical properties of the crystalline silicon material itself. Moreover, post-thermal treatment cooling is predominantly performed via natural, continuous cooling. This practice contributes to TID of τ within the silicon wafer, thereby potentially compromising the solar cell's photoelectric conversion efficiency [18,19].

This study investigates the impact of metallurgical isothermal cooling (the cooling curve is presented in Figure 2)—a heat treatment protocol widely employed in metallic materials [20] but hitherto unexplored in semiconductor photovoltaics—on the TID of τ in solar-grade Cz-Si. While isothermal cooling offers distinct process controllability—governed by isothermal temperature and hold time rather than cooling rate—it remains uninvestigated with respect to crystalline silicon photovoltaic performance. To bridge this gap, we conduct a systematic experimental study comparing τ evolution under isothermal versus continuous cooling protocols, thereby advancing the fundamental understanding and practical optimization of thermal processing for high-efficiency silicon solar cell fabrication.

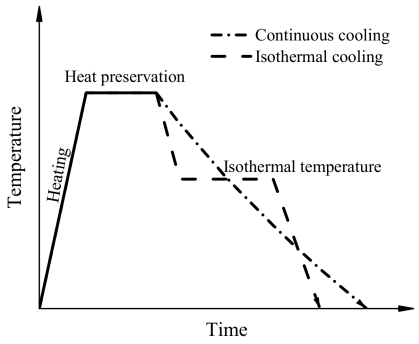


Figure 2. Continuous cooling and isothermal cooling curves of heat treatment.

2. Experiment Methods

2.1. Experimental Material

The silicon wafers employed in this study were p-type, boron-doped, Cz-Si wafers supplied by Jinko Solar (Shangrao, Jiangxi, China), exhibiting a resistivity of 3.0–3.5 Ω·cm and a nominal thickness of 180 μm. The total iron concentration—including both Fe_i and Fe in precipitates—was quantified using inductively coupled plasma mass spectrometry (ICP-MS) on a NexION5000G instrument (PerkinElmer, Waltham, MA, USA) for the same batch of wafers and found to be 2.0×10^{14} cm^{-3}. The $[Fe_i]$ was quantified independently using lifetime-based analysis, as detailed in the following section.

The experimental samples were diced into 18 mm × 18 mm square pieces. Subsequently, the silicon wafers underwent sequential cleaning: first, organic residue removal with acetone; second, chemical polishing using a 1:3 (v/v) mixture of 40% hydrofluoric acid (HF) and 70% nitric acid (HNO_3); and third, standard RCA cleaning. The cleaned wafers were then dried under a stream of high-purity nitrogen gas. Baseline characterization included measurement of τ on iodinepassivated samples. Only those wafers exhibiting comparable minority carrier lifetimes were selected for the subsequent experiments.

2.2. Thermal Processingof the Samples

Thermal processing was conducted in an RTP-500 rapid thermal processing furnace (East Star Applied Physics Institute, Beijing, China), featuring a sealed quartz process chamber heated by top-and-bottom halogen lamp arrays. Temperature control was implemented via a dual-loop feedback system, achieving a steady-state thermal stability of ±1 °C. Process sequencing and parameter execution were managed through a dedicated PC-based control interface. Silicon wafers were positioned horizontally on a quartz susceptor within the chamber, with three wafers processed per thermal cycle. The entire procedure was performed under a continuous purge of high-purity argon gas (≥99.999% purity) to ensure an oxygen-free, contaminant-suppressed ambient. The following thermal processing experiments were performed on the p-type Cz-Si wafers:

(1) Isothermal cooling experiments were conducted across a temperature range of 450–850 °C following heating at 900 °C in a high-purity argon atmosphere. As-received p-type Cz-Si wafers were processed in batches of three. Each batch underwent rapid heating to 900 °C, held isothermally for 20 min, then cooled at a controlled rate of 50 °C/s to one of nine target temperatures: 450 °C, 500 °C, 550 °C, 600 °C, 650 °C, 700 °C, 750 °C, 800 °C, or 850 °C. Upon reaching each target temperature, the wafers were held isothermally for 30 min before air cooling to ambient temperature (average cooling rate ≈ 30 °C/s). The representative isothermal cooling profile following heating at 900 °C is shown in Figure 3.

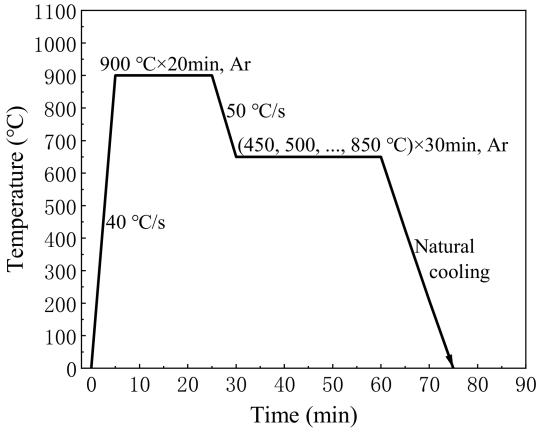


Figure 3. The thermal processing profile for p-type Cz-Si wafers: rapid heating to 900 °C in a high-purity argon atmosphere, held isothermally for 20 min, followed by controlled cooling to target temperatures (450 °C, 500 °C, 550 °C, 600 °C, 650 °C, 700 °C, 750 °C, 800 °C, and 850 °C), and subsequent isothermal holding at each temperature for 30 min before natural cooling to ambient temperature.

(2) Additional isothermal cooling experiments were conducted at 650 °C for varying durations following heating at 900 °C: As-received p-type Cz-Si wafers were processed in batches of three. Each batch was heated to 900 °C for 20 min under a high-purity argon atmosphere, then rapidly cooled at a controlled cooling rate of 50 °C/s to the target isothermal temperature of 650 °C—this temperature was selected based on prior optimization studies, as it yielded the maximum τ after stage (1) processing. Subsequently, samples were held at 650 °C for 0, 30, 60, 120, 180, and 240 min, respectively, and then allowed to cool to ambient temperature under natural convection conditions. The corresponding thermal profile for the isothermal ccooling step is shown in Figure 4.

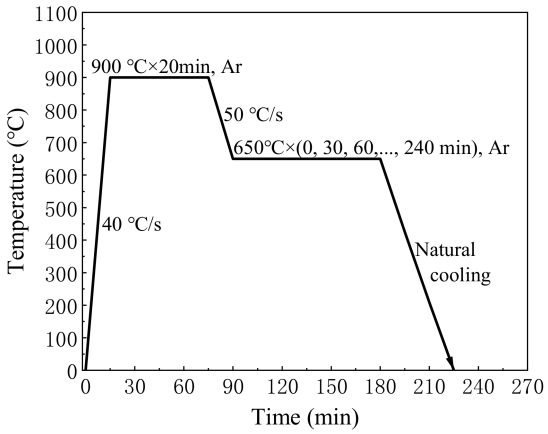


Figure 4. The thermal processing profile for p-type Cz-Si wafers: rapid heating to 900 °C in a high-purity argon atmosphere; held isothermally at 900 °C for 20 min; controlled cooling to 650 °C at 50 °C/s; and subsequent isothermal holding at 650 °C for 0, 30, 60, 120, 180, and 240 min respectively before natural cooling to ambient temperature.

Following thermal processing, the wafers were subjected to a 10 wt.% hydrofluoric acid (HF) etch to remove the native and thermally grown silicon dioxide layer. Subsequently, the samples were thoroughly rinsed with deionized water and dried under a stream of high-purity nitrogen gas (≥99.999% purity).

2.3. Analytical Testing Methods

The τ of the thermally processed silicon wafers was measured using a WT-2000PV lifetime tester (Semilab, Budapest, Hungary), based on the microwave-induced photoconductive decay (μ-PCD) technique [21], the τ measurements were performed using an infrared semiconductor laser pulse (wavelength: 905 ± 10 nm) as the excitation source. The optical injection fluence ranged from 1×10^{11} to 1.5×10^{13} phs/s [22]. The decaying conductivity can be monitored by detecting the microwave reflectivity. Prior to measurement, all samples were enclosed in a polyethylene bag with a small volume of 0.08 mol·L^{-1} iodine to enable insitu interfacial passivation. Iodine species chemisorb onto the silicon surface, saturating dangling bonds at the Si/ambient interface and thereby reducing the areal density of interface trap states. This passivation suppresses surface recombination velocity, thereby significantly reducing the impact of surface recombination on the τ.

The [Fe_i] was determined via lifetime-based analysis [13,22–24] using the Semilab WT-2000PV lifetime tester, which enables automated μ-PCD measurements. Under high-intensity illumination, FeB pairs dissociate, enabling sequential measurement of the τ prior to dissociation (τ_{before}) and following complete dissociation (τ_{after}). The [Fe_i] is subsequently calculated according to the following expression:

$$[Fe_i] = C_{\mu-PCD}\left(\frac{1}{\tau_{before}} - \frac{1}{\tau_{after}}\right) \quad (1)$$

where $C_{\mu-PCD} = 3.4 \times 10^{13}$ μs·cm^{-3}, a calibration constant derived from the effective excess carrier injection level under the instrument's standard measurement conditions [23].

3. Results and Discussion

3.1. Effect of Isothermal Temperatures on the τ and the [Fe_i]

Figure 5 depicts the dependence of the average τ on isothermal temperature for p-type Cz-Si wafers, error bars represent standard deviation (SD). As-received wafers underwent a heating at 900 °C in a high-purity argon ambient, followed by controlled isothermal holding across the temperature range of 450–850 °C, as detailed in Section 2.2 (1). For comparative context, the as-received average τ values for each wafer batch are superimposed on the plot. As evident from Figure 4, the average τ exhibits a substantial reduction relative to the as-received baseline. Notably, however, a clear nonmonotonic dependence is observed: τ increases progressively with rising isothermal temperature from 450 °C to 650 °C, reaches a maximum at 650 °C, and subsequently decreases upon further temperature increase.

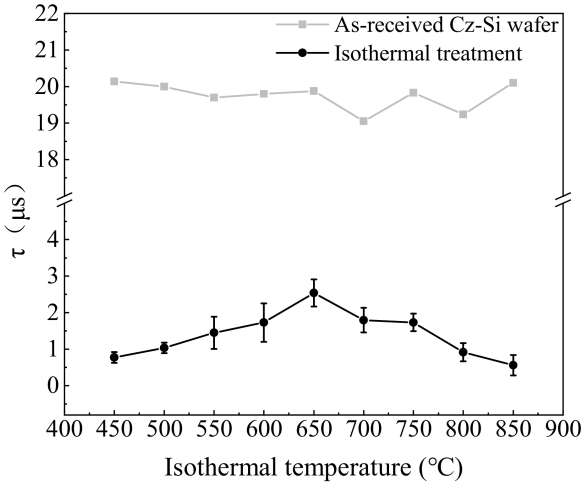


Figure 5. Variation in the average τ in p-type Cz-Si wafers with isothermal temperature, following heating at 900 °C. Isothermal treatment data are presented as mean ± SD, n = 3.

Figure 6 depicts the dependence of the average [Fe_i] on isothermal temperature in p-type Cz-Si wafers subjected to the aforementioned identical thermal treatment, together with the baseline [Fe_i] value measured in the as-received wafer. As evident from Figure 6, [Fe_i] exhibits a nonmonotonic trend with isothermal temperature: it decreases progressively from 450 °C, reaches a minimum at 650 °C, and then increases upon further elevation of the isothermal temperature. This nonmonotonic [Fe_i] trend is anti-correlated with the opposing nonmonotonic behavior of τ shown in Figure 5—where τ peaks at 650 °C while [Fe_i] reaches its minimum—which suggests a relationship between Fe_i accumulation and carrier recombination activity.

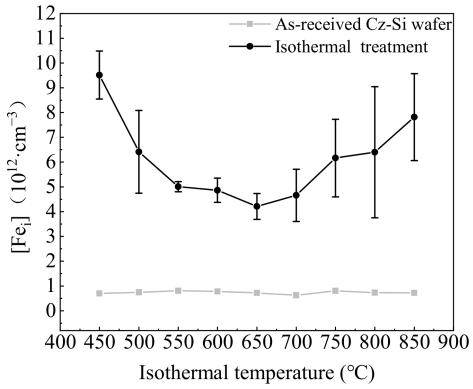


Figure 6. Variation in the average [Fe_i] in p-type Cz-Si wafers as a function of isothermal temperature, following heating at 900 °C. Isothermal treatment data are presented as mean ± SD, n = 3.

In this experiment, p-type Cz-Si wafers were subjected to heating at 900 °C. This treatment induced the dissolution of pre-existing iron precipitates and associated complexes, thereby releasing Fe_i into the silicon lattice. Using the established solubility expression for interstitial iron in silicon [2]—5×10^{22} cm^{-3} exp $(8.2 - 2.94\ eV/kT)$, valid for 900 °C < T < 1200 °C—the equilibrium [Fe_i] at 900 °C was calculated to be 4.3×10^{13} cm^{-3}. During subsequent isothermal cooling, these supersaturated Fe_i underwent re-precipitation, forming new iron-rich precipitates. To elucidate the isothermal temperature dependence of iron precipitation following the 900 °C anneal, Figure 7 was constructed by processing the data from Figure 6: specifically, the [Fe_i] measured at each isothermal temperature (Figure 6) was subtracted from the reference value of 4.3×10^{13} cm^{-3}, yielding the precipitated iron concentration ([Fe_p]) as a function of isothermal temperature.

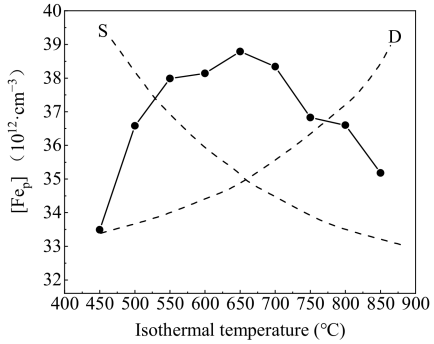


Figure 7. Variation in the average [Fe_p] in p-type Cz-Si wafers as a function of isothermal temperature, following heating at 900 °C.

Drawing on fundamental principles of physical metallurgy and precipitation theory, we interpret the experimental results shown in Figures 6 and 7 as follows. The kinetics of precipitate nucleation and growth during isothermal cooling are governed jointly by two

fundamental parameters: (i) the diffusion coefficient D of interstitial iron, which increases with temperature, and (ii) the supersaturation S of iron relative to its equilibrium solubility, which decreases with rising temperature. Consequently, at lower isothermal temperatures, precipitate formation is kinetically limited by sluggish diffusion; at higher temperatures, it is thermodynamically constrained by reduced supersaturation. The combined influence of these competing factors accounts for the nonmonotonic trends observed in the [Fe_i] (Figure 6) and [Fe_p] (Figure 7) as functions of isothermal temperature.

As noted in the Introduction, the minority carrier lifetime in crystalline silicon is critically determined by both the [Fe_i] and the microstructural attributes of iron precipitates—namely, their size, spatial distribution, and volumetric fraction. For wafers subjected to a 900 °C pre-anneal, isothermal holding at 650 °C represents the optimal thermal condition: under this regime, the opposing dependencies of iron diffusivity (D) and supersaturation (S) on temperature synergistically promote maximal precipitate growth, yielding the largest average precipitate size, the most localized spatial clustering (i.e., minimal dispersion), the lowest residual [Fe_i], and—consequently—the longest minority carrier lifetime. This temperature-dependent trade-off between kinetic facilitation and thermodynamic driving force governs the lifetime–interstitial iron relationship across all isothermal temperatures, not solely at 650 °C.

3.2. Effect of Isothermal Holding Time on the τ and the [Fe_i]

Figure 8 presents the average τ of p-type Cz-Si wafers as a function of isothermal holding time at 650 °C, error bars represent SD. All wafers underwent a heating step at 900 °C in a high-purity argon atmosphere, followed by isothermal holding at 650 °C for durations of 0, 30, 60, 120, 180, and 240 min, respectively, as outlined in Section 2.2 (2). For reference, the average τ values of the as-received wafers are shown as a light gray line. As shown in Figure 8, τ decreases substantially relative to the as-received baseline following the thermal protocol. Crucially, however, τ increases monotonically with isothermal holding time.

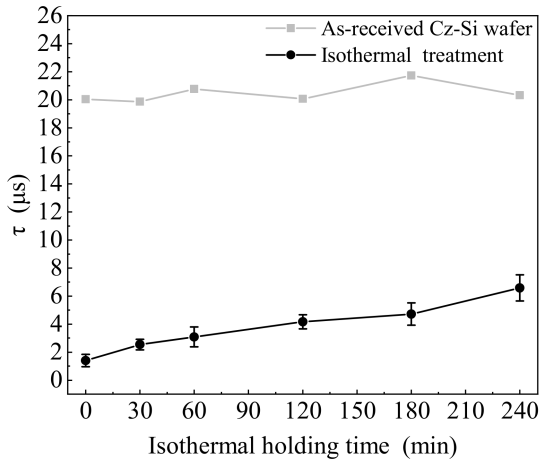


Figure 8. Variation in the average τ in p-type Cz-Si wafers with isothermal holding time at 650 °C, subsequent to a heating step at 900 °C. Isothermal treatment data are presented as mean ± SD, n = 3.

Figure 9 shows the evolution of average [Fe_i] in p-type Cz-Si wafers subjected to the identical thermal protocol described in Section 2.2 (2). Following this protocol, [Fe_i] increases substantially relative to the as-received baseline. The [Fe_i] declines monotonically with increasing isothermal holding time at 650 °C, asymptotically approaching the [Fe_i] level measured in the as-received material. This inverse temporal dependence—where [Fe_i] decreases while τ increases—constitutes robust experimental evidence linking interstitial iron accumulation directly to enhanced non-radiative recombination activity.

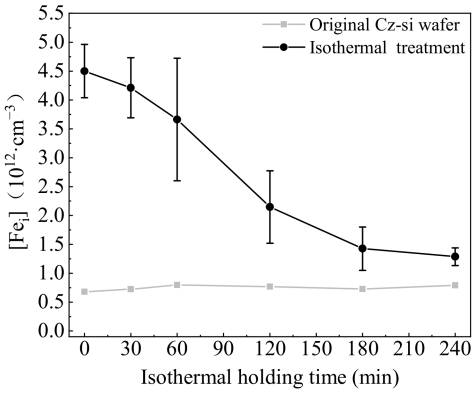


Figure 9. Variation in the average [Fe_i] in p-type Cz-Si wafers with isothermal holding time at 650 °C, following a heating step at 900 °C. Isothermal treatment data are presented as mean ± SD, n = 3.

A direct correlation is evident among τ, [Fe_i], and isothermal holding time, as illustrated in Figures 8 and 9. Following the high-temperature release of interstitial iron at 900 °C, subsequent isothermal holding at 650 °C induces interstitial iron precipitate evolution: with increasing hold time, [Fe_i] decreases markedly, while τ increases correspondingly. This behavior arises because 650 °C represents the thermodynamically favored nucleation and growth temperature for iron precipitates in silicon under the present experimental conditions—as identified in this study. According to the precipitation theory in physical metallurgy, at this temperature, extended isothermal holding promotes both an increase in precipitate number density and mean size, a reduction in spatial distribution, and a concomitant decrease in [Fe_i]. Collectively, these microstructural changes reduce the spatial density of electrically active recombination centers and enhance the τ.

As shown in Figures 8 and 9, although the [Fe_i] after 240 min of isothermal holding approaches that of the as-received sample, the τ remains markedly lower. This reflects the incomplete progression of iron precipitate coalescence: at 240 min, the extent of precipitate aggregation in silicon remains substantially below that of the as-received sample.

4. Conclusions

This study systematically examines the influence of metallurgical isothermal cooling parameters—specifically, isothermal temperature and isothermal duration—on [Fe_i] and minority carrier lifetime (τ) in p-type Cz-Si for photovoltaic applications. The key experimental findings are as follows: (1) Following a pre-anneal at 900 °C for 20 min, subsequent isothermal holding across a range of temperatures—followed by air cooling to ambient temperature—induces a pronounced increase in [Fe_i] and a concomitant decrease in τ, confirming the TID of minority carrier lifetime. (2) Under identical heating conditions, variation in the isothermal temperature reveals a distinct extremum behavior: [Fe_i] decreases monotonically with rising temperature in the low-temperature regime (≤650 °C), reaching a minimum at 650 °C; τ exhibits the inverse trend, peaking at the same temperature. Above 650 °C, [Fe_i] increases and τ declines, indicating diminished precipitation efficiency due to enhanced iron solubility and reduced driving force for nucleation. (3) Isothermal holding at 650 °C maximizes iron precipitation, thereby minimizing [Fe_i] and maximizing τ. This optimum arises from the balanced interplay between the diffusion coefficient (D) of interstitial iron in silicon and its supersaturation ratio (S), which jointly govern nucleation kinetics and precipitate growth. (4) When the isothermal holding is conducted at 650 °C for durations of 0, 30, 60, 120, 180, and 240 min, [Fe_i] decreases monotonically and τ increases correspondingly—demonstrating time-dependent evolution toward thermodynamic equilibrium. Collectively, these results establish isothermal cooling—not as a mere alternative,

but as a strategically controllable process step—for mitigating minority carrier lifetime degradation during crystalline silicon solar cell fabrication. Compared with conventional continuous cooling, deliberate isothermal holding enables the precise manipulation of iron precipitation kinetics. The optimal isothermal temperature is determined by the intersection of kinetic accessibility (governed by D) and thermodynamic favorability (governed by S), with 650 °C identified as the experimentally robust setpoint; longer isothermal durations further increase τ, subject to throughput and thermal budget constraints.

Author Contributions: Conceptualization, P.Z., K.W., Y.Z. and L.Z.; Methodology, P.Z., K.W. and Y.Z.; K.W. and P.Z.; Investigation, P.Z. and K.W.; Resources, P.Z. and L.Z.; Data curation, Y.Z.; Writing—original draft, P.Z.; Writing—review & editing, K.W. and L.Z.; Visualization, P.Z. and Y.Z.; Supervision, P.Z.; Project administration, P.Z.; Funding acquisition, P.Z. All authors have read and agreed to the published version of the manuscript.

Funding: This research was funded by Nanchang Institute of Science and Technology Special Research Project grant number NGMBZX-26-03; Nanchang Institute of Science and Technology Special Fund for Talents grant number NGRCZX-25-04.

Data Availability Statement: The original contributions presented in this study are included in the article. Further inquiries can be directed to the corresponding author.

Conflicts of Interest: The authors declare no conflict of interest.

References

1. Yang, D. *Solar Cell Materials*; Chemistry Industry Press: Beijing, China, 2006; pp. 104–141.
2. VDMA, e.v. *Photovoltaic Equipment. International Technology Roadmap for Photovoltaic (ITRPV), Results 2020*, 12th ed.; VDMA: Frankfurt, Germany, 2021.
3. VDMA, e.v. *Photovoltaic Equipment. International Technology Roadmap for Photovoltaic (ITRPV), Results 2025*, 17th ed.; VDMA: Frankfurt, Germany, 2026.
4. Wang, W.; Li, H.; Zhou, C.; Zhao, L. *Manufacturing Technology of Crystalline Silicon Solar Cells*; China Machine Press: Beijing, China, 2013; p. 19.
5. Zhou, P.; Ke, H.; Zhou, L. Effect of heat treatment and cooling rate on minority carrier lifetime of Czochralski silicon. *Trans. Mater. Heat Treat.* **2012**, *33*, 23–27.
6. Buonassisi, T.; Istratov, A.A.; Marcus, M.A.; Lai, B.; Cai, Z.; Heald, S.M.; Weber, E.R. Engineering metal-impurity nanodefects for low–cost solar cells. *Nat. Mater.* **2005**, *4*, 676–679. [CrossRef] [PubMed]
7. Rohatgi, A.; Rai-Choudhury, P. *Defect and Carrier Lifetime in Silicon*; American Society for Testing and Materials: West Conshohocken, PA, USA, 1983; pp. 389–404.
8. Xi, Z.; Yang, D.; Chen, J.; Wang, X.; Wang, L.; Que, D.; Moeller, H.J. Iron precipitation in crystalline silicon. *Chin. J. Semicond.* **2003**, *24*, 1166–1170.
9. Olikh, O.; Zavhorodnii, O. Iron's impact on silicon solar cell execution: Comprehensive modeling across diverse scenarios. *Mater. Sci. Eng. B* **2025**, *317*, 118192. [CrossRef]
10. Al-Ani, O.A.; Goss, J.P.; Briddon, P.R.; Rayson, M.J.; Cowern, N.E.B. Interstitial Fe-pairs in silicon. *J. Cryst. Growth* **2017**, *468*, 54–56. [CrossRef]
11. Wünstel, K.; Wagner, P. Interstitial iron and iron-acceptor pairs in silicon. *Appl. Phys. A* **1982**, *27*, 207–212. [CrossRef]
12. Istratov, A.A.; Hieslmair, H.; Weber, E.R. Iron and its complexes in silicon. *Appl. Phys. A* **1999**, *69*, 13–44. [CrossRef]
13. Istratov, A.A.; Hieslmair, H.; Weber, E.R. Iron contamination in silicon technology. *Appl. Phys. A* **2000**, *70*, 489–534. [CrossRef]
14. Weber, E.R. Transition metals in silicon. *Appl. Phys. A* **1982**, *30*, 1–22. [CrossRef]
15. Brotherton, S.D.; Bradley, P.; Gill, A. Iron and the iron-boron complex in silicon. *J. Appl. Phys.* **1985**, *57*, 1941–1943. [CrossRef]
16. Nilsson, S.G.; Kleverman, M.; Emanuelsson, P.; Grimmeiss, H.G. Identification of the iron-boron line spectrum in silicon. *Mater. Sci. Forum* **1994**, *143–147*, 171–175. [CrossRef]
17. Gehlhoff, W.; Irmscher, K. EPR Identification of the Different Charge States of the Iron–Acceptor Pairs in Silicon. *Solid State Phenom.* **1993**, *32*, 219–224. [CrossRef]
18. Zhou, L. Thermal engineering of crystalline silicon and solar cell processes. In Proceedings of the 2nd Total Energies Science Forum–Advanced Solar Cell Technology, Suzhou, China, 3 June 2001.

19. Wang, P.; Zhang, Y.; Ou, Z.; Wang, Z.; Chen, Z.; Lin, Y. Bulk-Defect Dominated Minority Carrier Degradation: Mechanisms and Suppression Strategies for High-Temperature Behavior of Photovoltaic n-Type Czochralski Silicon Wafers. *J. Synth. Cryst*. **2026**, *55*, 619–626.
20. Carlos, P.B. *Physical Metallurgy and Heat Treatment of Steel*; Springer Nature: Berlin/Heidelberg, Germany, 2023; p. 49.
21. Schmidt, J.; Aberle, A.G. Accurate method for the determination of bulk minority–carrier lifetimes of mono and multicrystalline silicon wafers. *J. Appl. Phys*. **1997**, *81*, 6186–6199. [CrossRef]
22. Semiconductor Physics Laboratory, Co., Ltd. *WT–2000PV User Manual*; Semiconductor Physics Laboratory, Co., Ltd.: Budapest, Hungary, 2024.
23. Zoth, G.; Bergholz, W. A fast preparation-free method to detect iron in silicon. *J. Appl. Phys*. **1990**, *67*, 6764–6771. [CrossRef]
24. Rost, M.; Stichtenoth, D.; Meyer, K. Iron detection in crystalline silicon by different lifetime measurement techniques. *Energy Procedia* **2015**, *77*, 159–169. [CrossRef]

Disclaimer/Publisher's Note: The statements, opinions and data contained in all publications are solely those of the individual author(s) and contributor(s) and not of MDPI and/or the editor(s). MDPI and/or the editor(s) disclaim responsibility for any injury to people or property resulting from any ideas, methods, instructions or products referred to in the content.